Time-Frequency Analysis of Rocket Nozzle Wall Pressures during Start-up Transients

Woutijn J. Baars[1], Charles E. Tinney[1] and Joseph H. Ruf[2]

[1]The University of Texas at Austin, Austin, TX, 78712, USA

[2]NASA Marshall Space Flight Center, Huntsville, AL, 35812, USA

E-mail: `baars@mail.utexas.edu`

Abstract. Surveys of the fluctuating wall pressure were conducted on a sub-scale, thrust-optimized parabolic nozzle in order to develop a physical intuition for its Fourier-azimuthal mode behavior during fixed and transient start-up conditions. These unsteady signatures are driven by shock wave turbulent boundary layer interactions which depend on the nozzle pressure ratio and nozzle geometry. The focus however, is on the degree of similarity between the spectral footprints of these modes obtained from transient start-ups as opposed to a sequence of fixed nozzle pressure ratio conditions. For the latter, statistically converged spectra are computed using conventional Fourier analyses techniques, whereas the former are investigated by way of time-frequency analysis. The findings suggest that at low nozzle pressure ratios –where the flow resides in a Free Shock Separation state– strong spectral similarities occur between fixed and transient conditions. Conversely, at higher nozzle pressure ratios –where the flow resides in Restricted Shock Separation– stark differences are observed between the fixed and transient conditions and depends greatly on the ramping rate of the transient period. And so, it appears that an understanding of the dynamics during transient start-up conditions cannot be furnished by a way of fixed flow analysis.

1. Introduction

A persistent difficulty to developing statistical models of transient phenomena is simply the suitability of the analysis technique selected. For stationary systems the approach is much more straightforward with results being generated using ensemble averages of long time series. In transient systems however, the non-stationarity of the mean signal is much more challenging to handle as it requires that the time-dependence be preserved during the analysis. This is particularly difficult as the time scales associated with the important features in the signal reside on the same order of the period in which the transient phenomena occur.

Most conventional methods used for analyzing time series use some form of a harmonic decomposition in order to view the energy content per frequency. For transient data, time-frequency analysis is the only suitable mathematical technique as it performs the energy decomposition in time-frequency space; *surprisingly, most applications of this technique are to stationary data.* The motive of time-frequency analysis is to search for localized singularities, or regions in the time series, with unique spectral content. Such information is otherwise de-localized, *i.e.* spread out, when conventional harmonic analysis techniques are applied. Joint time-frequency distributions or wavelet transforms provide the mathematical framework for

performing the time-frequency analysis and have been studied extensively by Cohen (1989) and Farge (1992), respectively.

One such example, where transients features are an important part of the entire process, is observed during the start-up and shut-down cycle of Thrust-Optimized Parabolic (TOP) contoured rocket nozzles, as are found on modern liquid propellant engines. During the start–up and shut–down cycle of TOP nozzles, the flow on the interior surface of the nozzle undergoes a lifecycle of events, each of which depends greatly on the Nozzle Pressure Ratio (NPR) and nozzle geometry (Frey & Hagemann, 2000; Nguyen *et al.*, 2003; Ruf *et al.*, 2009; Baars *et al.*, 2011). At low NPR, the flow state is characterized by Free Shock Separation (FSS) while at higher NPR, the flow transitions to Restricted Shock Separation (RSS). Illustrations of these two uniquely different states are depicted in figure 1, taken from Baars *et al.* (2011). The first of these, FSS, occurs at low NPRs, is characterized by an incipient separation of the flow along the interior surface of the nozzle, and is triggered by an adverse pressure gradient between the region of isentropic expansion and the subsonic entrainment region. Compression waves coalesce to form a separation shock whose foot resides at the point of flow separation. In general, this separation shock is asymmetric thus producing excessive thermal and lateral loads acting on the nozzle wall. Additional interactions develop between this separation shock and a reflected shock; the reflected shock originates from the triple-point which is the location where the Mach disk, internal and reflected shocks coincide. A separated region encompassing a series of compression and expansion waves forms downstream of the separated shock and away from the nozzle wall (identified in figure 1a as a detached supersonic plume). At lower NPRs, this separated flow fails to reattach to the nozzle wall and so the flow continues as a free supersonic jet until it eventually diffuses far downstream. Between the detached supersonic plume and the nozzle wall, a recirculating region forms which entrains low-speed ambient flow along the nozzle wall. A profile of the static wall pressure p_w/p_a is shown in figure 2a taken from Ruf *et al.* (2009) and Baars *et al.* (2011). This profile indicates a regular expansion up to the incipient separation point, thereafter, a rise to near ambient pressure is observed throughout the entire subsonic entrainment region.
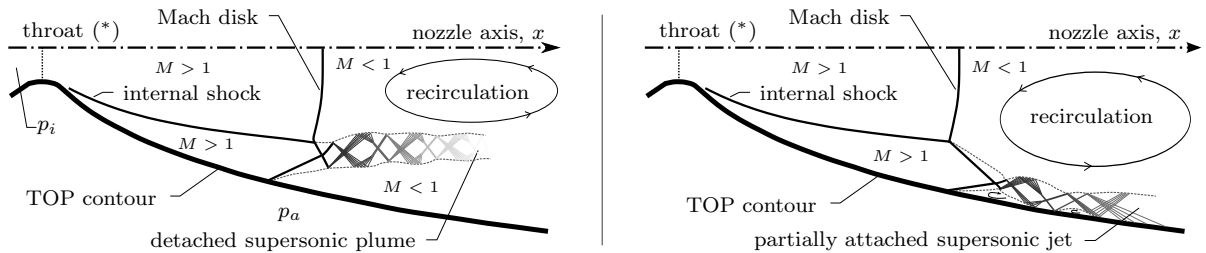

Figure 1. Illustration of the internal shock structure during a Free Shock Separation (FSS) state *(left)* and a Restricted Shock Separation (RSS) state *(right)* in a TOP nozzle - extracted from Baars *et al.* (2011).

As the NPR in a TOP nozzle continues to increase, an abrupt transition from FSS to RSS states occurs during which the incipient separation point pushes downstream and aft of the Mach disk. This generates outward radial momentum fluid which forces the detached supersonic plume to reattach to the nozzle wall as shown in figure 1. A bounded region of separated flow forms between the separation shock and an expansion fan reflecting from the shear layer of the supersonic plume; this is referred to as an annular separation bubble. Depending on the NPR, the annular supersonic jet might remain attached to the wall. However, it is believed that if the initial shocks are sufficiently strong, an additional shock (emanating from the wall) will form which will separate the flow from the inner wall through a Shock-Wave Turbulent Boundary

Layer Interaction (SWTBLI). Presumably, the flow will reattach further downstream, thereby creating a second bounded annular separation bubble; see figure 2b,c. These annular separation bubbles may interact with one another and cause additional amplification or cancellation of the initial off-axis loads acting on the nozzle wall. Upon further increases in NPR, the RSS structure returns to a FSS state, which eventually vanishes once the nozzle flows full.
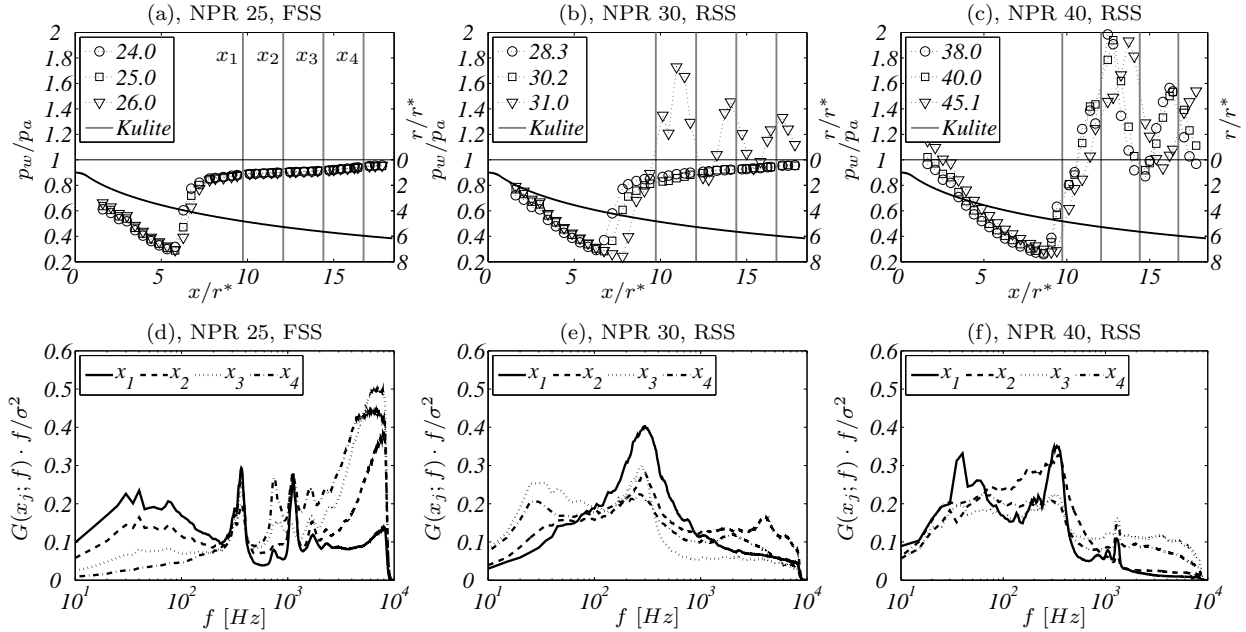

Figure 2. (a) - (c) Static wall pressure distributions for the nominal, and surrounding, constant NPR conditions. (d) - (f) Frequency spectra of the fluctuating wall pressures at each of the four axial stations - extracted from Baars *et al.* (2011).

A typical approach for developing a statistical characterization of this transient flow is to acquire long data sets at fixed NPR conditions along the transient start-up period. However, to date, there has been no investigation focused on determining whether such an approach is satisfactory. That is, can a satisfactory understanding of the dynamical characteristics relating to the internal flow and fluctuating wall pressure footprint during transient operation of an overexpanded nozzle be furnished by way of fixed flow (NPR) analysis (Nguyen *et al.*, 2003). As an example, the one-sided power spectral density of the fluctuating wall pressure at three constant NPR conditions (25, 30 & 40) is shown in figure 2d-f, taken from Baars *et al.* (2011). It is clear from these figures that the dynamical features are truly complex, with a unique spectral shape at each NPR condition. The objective of this paper is to compare the spectral footprints for fixed and transient nozzle operation to verify whether the transient cycle (fluctuations superposed a transient mean flow) can be studied by analyzing a sequence of fixed point flow conditions along the transient cycle (fluctuations superposed a steady mean flow).

2. Experimental Arrangement

2.1. Facility and Instrumentation

The experimental campaign was conducted in the Nozzle Test Facility (NTF) at NASA MSFC in Spring 2008 (Ruf *et al.*, 2009). The cold-flow tests were performed using an axisymmetric sub-scale nozzle that was mounted inside a vacuum chamber and exhausted into an ejector pipe.

Start-up transients and steady NPR conditions were achieved by decreasing the vacuum chamber pressure while maintaining a constant plenum pressure and temperature of $9.2atm$ ($135psia$) and $340K$, respectively. The nozzle has a TOP contour and was designed to simulate the separated flow behavior observed during the transient start-up of the Space Shuttle Main Engine (SSME). The throat radius of the nozzle is $r^* = 19.05mm$ ($0.75in$) and has an exit-to-throat area ratio of 38. A schematic of the nozzle assembly with relevant coordinates is shown in figure 3.

Axial and azimuthal arrays of pressure transducers were used to measure the static and fluctuating wall pressure signatures on the interior surface of the nozzle. This consisted of two curvilinear arrays (nominally at $\theta = \pm\pi/2$) of 37 static pressure ports along the axial direction with constant axial spacings of $\Delta x/r^* = 0.45$. These static pressure ports spanned between $x/r* = 1.60$ and 17.80; the exit plane of the nozzle is located at $x/r^* = 18.40$. The static wall pressures were sampled at $500Hz$ and averaged over $0.25s$ intervals. As for the fluctuating wall pressure signatures, a total of 32 high-frequency Kulite XT-140 transducers, mounted flush along the expanding surface of the nozzle, were sampled simultaneously at a sampling frequency of $f_s = 20,480Hz$. The arrangement of the transducers comprised four axial stations, $x/r^* = 9.73, 12.07, 14.40, 16.73$ (further referred to as x_j, $j = 1...4$), with each axial station comprising an azimuthal array of eight transducers with equal increments of $\Delta\theta = 45°$ (θ_i, $i = 1...8$). For this analysis, the fluctuating wall pressure has not been scaled to account for decreases in ambient pressure using this vacuum chamber facility (constant in reality); caution should be exercised when comparing absolute quantitative results between NPRs.

2.2. Experimental Conditions

This analysis was separated into two primary categories: (1) Transient NPR (start-up, $dNPR/dt > 0$) and (2) Fixed NPR conditions. For the transient conditions, three ramping rates were considered (ramp 1-3) and are shown in figure 3. Ramp 1 has the fastest start-up for the region NPR < 40 with a maximum rate of $dNPR/dt \approx 25s^{-1}$. Ramps 2 and 3 comprise ramp rates that are roughly $10s^{-1}$ and $8s^{-1}$ for NPR < 35, that increase to $50s^{-1}$ by NPR 55.
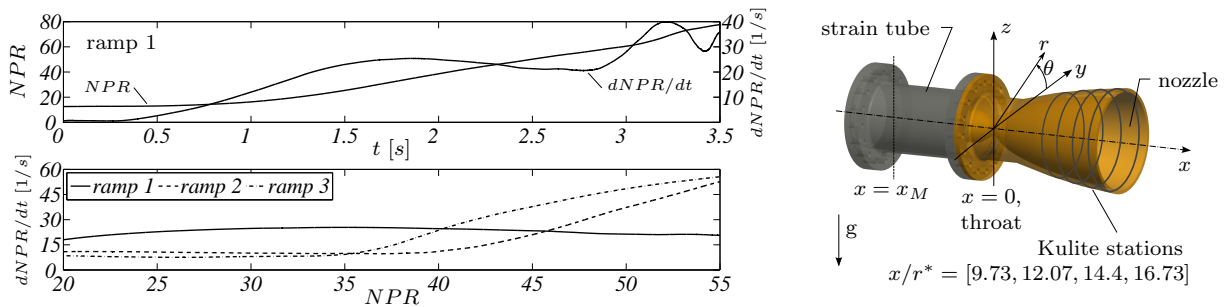

Figure 3. *(top left)* NPR(t) and ramp rate $dNPR/dt(t)$ for the first start-up transient. *(bottom left)* Ramp rate versus NPR for three start-up transients. *(right)* The sub-scale nozzle assembly.

Fixed flow conditions are considered for NPR set points of 25, 30, 40 and 50 encompassing both FSS and RSS flow states. For these fixed NPR runs, data was acquired for 18 seconds to allow good statistical convergence. A discussion of the static and fluctuating wall pressure characteristics during fixed NPR conditions can be found in Baars *et al.* (2011). Facility-induced disturbances were detected in these fixed NPR studies and are believed to be related to (1) the close proximity of the ejector pipe to the nozzle exit plane, and (2) acoustic/aerodynamic resonance in the closed vacuum chamber. Research is currently being conducted in a fully anechoic environment at The University of Texas at Austin to quantify the effects of these facility disturbances.

3. Fourier-Azimuthal Decomposition of the Fluctuating Wall Pressure

Given the azimuthal spatial configuration of the fluctuating wall pressure transducers, it appeared more straightforward to analyze these signals in terms of their Fourier-azimuthal mode coefficients. This was achieved by Fourier transforming the original high-frequency pressure field, $p(x, \theta, t)$, in azimuth in order to obtain time-dependent Fourier-azimuthal coefficients

$$p\left(x; m'; t\right) \in \mathbb{C}, \quad p\left(x; m'; t\right) = \mathcal{F}\left[p\left(x, \theta, t\right)\right]_\theta, \tag{1}$$

where m' indicates the mode number. Recall that for both positive ($m' = 1, 2, 3$) and negative ($m' = -1, -2, -3$) mode numbers, the complex Fourier coefficients occur as conjugate pairs, i.e. $p(x; m' = 1; t) = p^*(x; m' = -1; t)$, while for $m' = 0, 4$ these coefficients are real. In the remainder of the paper the real ($m > 0$) and imaginary ($m < 1$) part of the Fourier coefficients $m' = 0, 1, 2, 3, 4$ are considered and are denoted as

$$p\left(x; m; t\right) \in \mathbb{R}, \quad m = 0, 1, -1, 2, -2, 3, -3, 4. \tag{2}$$

These 'mode coefficients' represent the amplitude of the physical modes that are illustrated in figure 4. The strength of this decomposition is that variations in azimuth are now studied in terms of these periodic modes and only the first mode is responsible for off-axis force generation in the $x-$ and $y-$direction for $m = 1$ and $m = -1$, respectively.
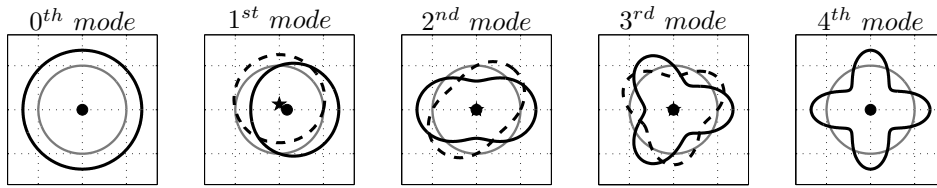

Figure 4. Physical interpretation of the Fourier-azimuthal decomposition. Solid and dashed lines correspond to the real ($m > 0$) and imaginary ($m < 0$) parts of the Fourier coefficients.

A first step to comparing the dynamical characteristics between the transient and fixed NPR conditions is to compare the total resolved energy in the mode coefficients at each axial station, x_j. This is computed for the temporal domain k as follows

$$\Lambda_k(x_j) = \sum_m \lambda_k^{(m)}\left(x_j\right), \tag{3}$$

where $\lambda_k^{(m)}\left(x_j\right)$ is the variance of the time-dependent mode coefficient $p\left(x_j; m; t\right)$ and $t \in k$. Fractions of resolved-energy per mode are determined using

$$\alpha_k(x_j; m) = \frac{\lambda_k^{(m)}\left(x_j\right)}{\Lambda_k(x_j)}. \tag{4}$$

The temporal domain k used to compute $\alpha_k(x_j; m)$ for the transient data is associated with windows centered around NPR set points of 25, 30, 40, & 50 (corresponding to the fixed NPR conditions) and are 1 NPR in width. As for fixed NPR conditions, the complete time series (18 seconds) is used.

The time-series of the breathing mode coefficients ($m = 0$) at the third axial station are presented in figure 5 for all three ramping conditions. Eigenspectra (limited to mode $m = 0$ and $m = 1$) are also shown for transient and fixed nozzle operation. A non-trivial result of all
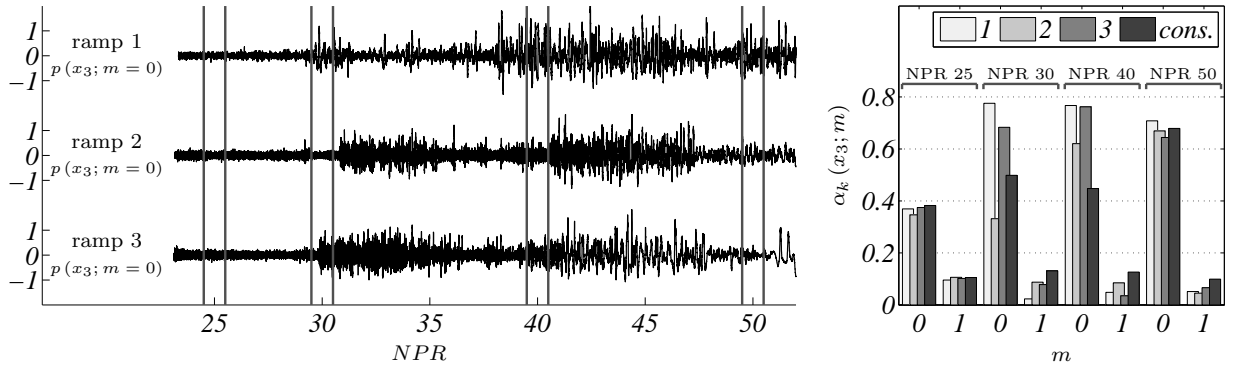
Figure 5. *(left)* Breathing mode coefficients ($m = 0$) at axial station x_3 in $\left[\times 10^5 Pa\right]$ as function of NPR for the three ramps (high-pass filtered for $f = 10Hz$), *(right)* Scaled eigenspectra of the Fourier modes $m = 0$ and $m = 1$ for the start-ups (1-3) and the fixed NPR runs (cons.).

cases investigated is that the breathing mode dominates the energy wavenumber spectrum of the fluctuating surface pressure. During FSS state at NPR 25, the mode energy fractions are in agreement for all transients and fixed operations. The FSS → RSS transition in the nozzle occurs at different NPRs (close to NPR 30) for the three transients as is observed by a sudden increase in amplitude of the mode coefficients. Therefore, the energy spectra are inconsistent for the various ramped and fixed NPR cases during NPR 30. At NPR 40, a shock-induced separation occurs (Baars *et al.*, 2011) whose shock foot resides close to axial station x_3. The breathing mode energy fraction is now under predicted by the steady case and, as a consequence, the energy fraction in the side-load inducing mode $m = 1$ is higher. The modal energy fractions at the location of flow reattachment (NPR 50, x_3) match well for the transient versus fixed operation.

4. Time-Frequency Analysis of the Pressure Modes

Joint time-frequency analysis, or wavelet transforms, allows the spectral energy of a transient signal to be determined as a function of time and is performed here to extract spectral content from the transient Fourier-azimuthal more coefficients. A more thorough review of these methods can be found in Cohen (1989) and Farge (1992), respectively. In this study, the continuous wavelet transform is applied to the real-valued pressure mode coefficients, which is here described.

4.1. Morlet Wavelet Transform
During wavelet analyses, an *a priori* known function (the mother wavelet) is temporally convolved with the signal. This convolution is performed at various time-scales l, i.e. frequencies, and so decomposes the signal in time-frequency space. The progressive complex-valued Morlet wavelet, Eq. (5), is used as the mother wavelet since energy density and phase can be extracted and because a higher resolution in frequency can be achieved when compared to other wavelets.

$$\psi\left(t/l\right) = e^{j\omega_\psi t/l}e^{-\left|t/l\right|^2/2} \qquad (5) \qquad \hat{\psi}\left(l\omega\right) = \left(2\pi\right)^{-1/2} e^{-\left(l\omega - \omega_\psi\right)/2} \qquad (6)$$

The Morlet wavelet comprises a simple plane wave whose amplitude is modulated by a Gaussian function. The non-dimensional frequency is taken as $\left|\omega_\psi\right| = 6$. Both the Morlet wavelet and its transform, Eq. (6), are shown in figure 6.
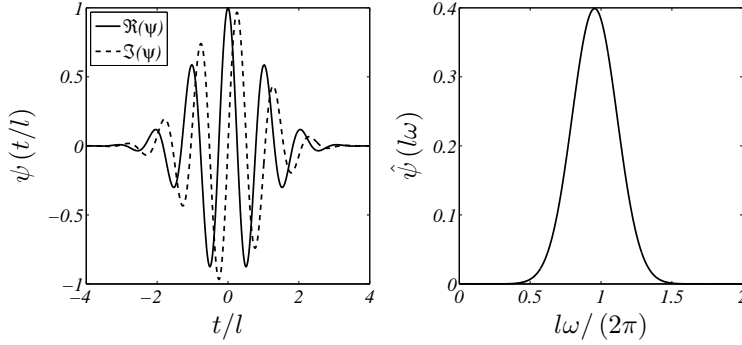
Figure 6. *(left)* The Morlet wavelet $\psi \in \mathbb{C}$ in the time domain and *(right)* in the frequency domain.

The temporal convolution of the Morlet wavelet with the pressure mode coefficients results in complex-valued wavelet coefficients $\tilde{p}(x; m; l, t)$, defined as

$$\tilde{p}(x; m; l, t) = \int p(x; m; t') \psi^* \left(\frac{t' - t}{l} \right) dt, \tag{7}$$

with the convolution being performed in the frequency domain (Farge, 1992). The wavelets are mutually similar between various scales to ensure similar influence on the coefficients. This results in a relatively low temporal resolution at large scales (low freq.) followed by a higher temporal resolution at small scales. Moreover, the resolution in time-frequency space involves a trade-off since a finer resolution in time is associated with a coarser resolution in frequency and vice versa. In the current analysis, frequencies are resolved in the range of $10Hz < f < f_s/2$ using a base-2 logarithmic progression of 81 scales in order to achieve a uniform grid on a logarithmic frequency scale. The energy density is now given by

$$E(x; m; l, t) = \frac{|\tilde{p}(x; m; l, t)|^2}{l}, \tag{8}$$

and is known as the local wavelet spectrum. Finally, the wavelet scale is transformed to the equivalent Fourier frequency, i.e. $E(x; m; l, t) \rightarrow E(x; m; f, t)$. The local wavelet spectrum of a sample pressure coefficient $p(x_3; m = 0; t)$ during fixed NPR 40 conditions is shown in figure 7(*left*)[1].

Trigonometric basis functions (no decay to zero) are used in the creation of Fourier spectra which are therefore de-localized (transient data cannot be analysed), as opposed to the localized wavelet analysis (Farge, 1992). Nonetheless, Fourier analyses is suitable and convenient for steady signals where there are no concerns for a temporally evolving mean signal. The Fourier spectrum, in terms of the one-sided power spectral density $G(x; m; f)$, is presented in non-dimensional form $G(x; m; f) \cdot f/\sigma^2$, where σ^2 is the signal's variance. For wavelet analyses, when time-scales of transient events are small or steady signals are considered, time-averaged wavelet spectra can be created following $\overline{E} = 1/T \int_T E \, dt$. For the steady signal, a global wavelet spectrum ($T = length\ of\ signal$) shows good agreement with the Fourier spectrum; see figure 7(*right*).

4.2. Influence of Transient Start-up Rate on Time-Frequency Distribution
One of the larger side load events that occurs during the transient start-up of overexpanded TOP nozzles occurs when the shock pattern transitions from FSS $\rightarrow$ RSS state (Hagemann

---

[1] Overlapping signal partitions of $N = 2^{14}$ samples are wavelet transformed. The regions inside the cone of influence (Farge, 1992), for $10Hz < f < f_s/2$, are presented in a continuous fashion throughout the paper.
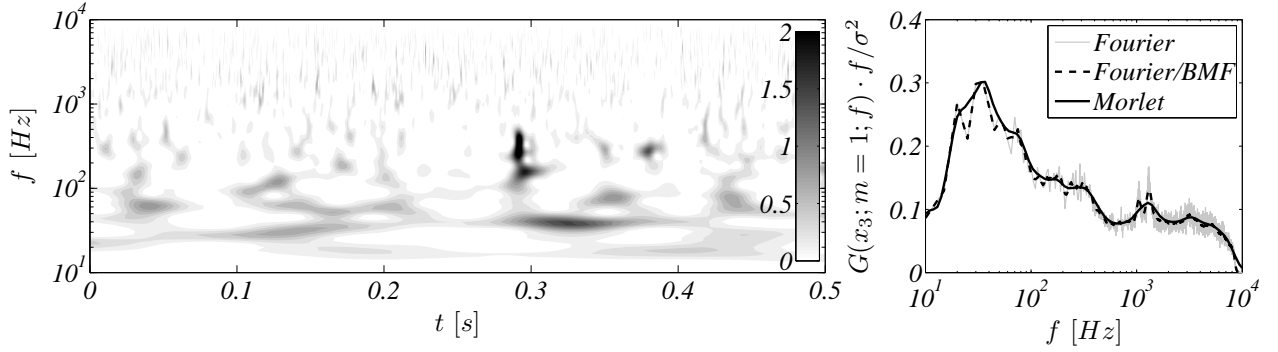
Figure 7. *(left)* Local wavelet spectrum, $E(x_3; m = 1; f, t) \cdot f$, in $[\times 10^{12} Pa^2]$ of the steady NPR 40 condition, *(right)* Comparison of the global wavelet spectrum and the Fourier spectrum (both computed from $18s$ of data) - a 5% bandwidth moving filter is applied to 'Fourier/BMF'.

et al., 2002; Ruf *et al.*, 2009). Therefore, the local wavelet spectra of the side-load inducing mode $m = 1$, station x_3, are presented for a NPR domain encompassing transition (figure 8). From the time-series and wavelet spectra it is observed that higher fluctuations occur for slower ramping rates (after transition). Most energy is present for $f \lesssim 600Hz$ for all ramps. Moving now to ramping rates 2 & 3, most energy is present in the range $60Hz < f < 600Hz$ just after transition, while a short duration later ($NPR > 33$) the energy is moved to lower frequencies.
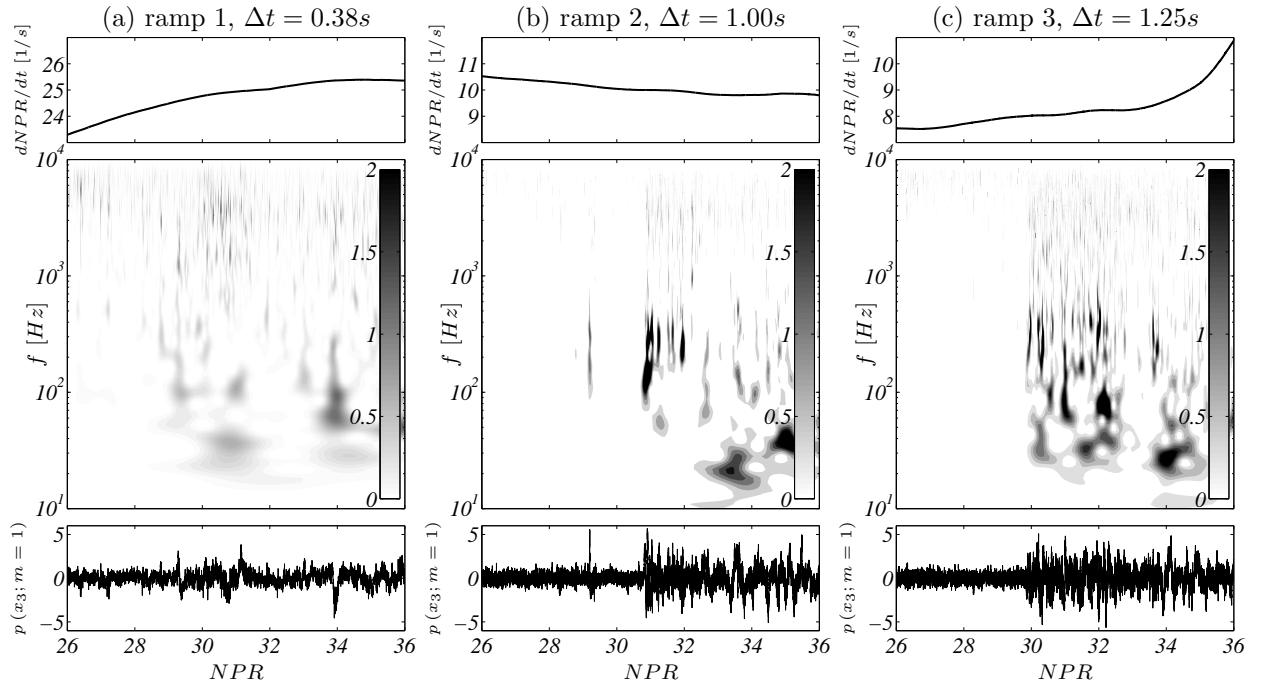

Figure 8. Local wavelet spectrum, $E(x_3; m = 1; f, t) \cdot f$, in $[\times 10^{12} Pa^2]$ as function of NPR. The ramp rate and raw time signal in $[\times 10^4 Pa]$ (high-pass filtered for $f = 10Hz$) are synchronously shown. Δt is the duration associated with the NPR range.

4.3. Comparing Spectral Characteristics: Fixed versus Transient

The underlying objective of this study is to investigate whether the spectral behavior of the pressure modes, as observed during fixed nozzle operations, reflect the same dynamical characteristics observed during transient operation. The local wavelet spectrum of mode coefficient $p(x_3; m = 1; t)$ is shown in figure 9(*left*) for the highest ramp rate. From this, several instantaneous spectra at NPR 25 and 40 are created by time-averaging the local wavelet spectra over four different window widths centered on the NPR set points. This is shown in figure 9(*middle,right*) to demonstrate the sensitivity of the time-frequency analysis to different window widths. During FSS at NPR 25, the instantaneous spectra are in good agreement. Much larger variations in spectral content occur when the flow is in RSS state. The window size is shown here to have a direct influence on the instantaneous spectra and demonstrates how even modest amounts of temporal averaging can have a profound influence on the resultant spectra.
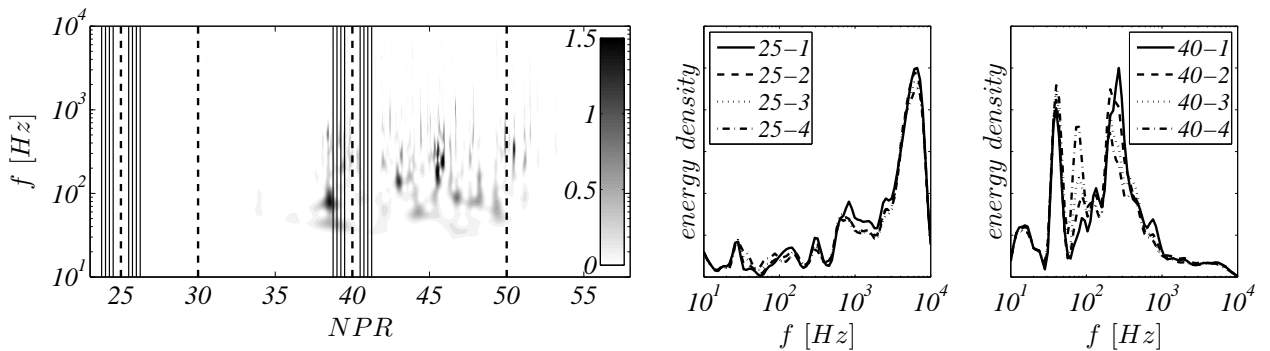

Figure 9. *(left)* Local wavelet spectrum, $E(x_3; m = 1; f, t) \cdot f$, in $[\times 10^{13} Pa^2]$ as function of NPR (ramp 1), $\Delta t = 1.48s$, *(middle,right)* The instantaneous spectra at the NPR set point of 25 and 40 for four different windows (1-4) that span 1, 1.5, 2 and 2.5 NPR.

Instantaneous spectra corresponding to NPR set points (25, 30, 40 & 50) are shown in figure 10 for all three ramping rates using a window width of 2 NPR. At NPR 25, the ramping rate appears to have little influence on the fluctuating wall pressure structure; albeit, the transducers are located in the subsonic entrainment regions of the flow. At higher NPR (30, 40, 50), the spectral distribution is highly sensitive to dNPR$/dt$. In figure 11 the global wavelet spectra are overlaid the Fourier spectra for the fixed NPR conditions using the same Fourier-azimuthal mode and axial station $(m = 1, x_3)$. A visual comparison of the two suggests that steady operation at NPR 25 (FSS) reflects the same spectral characteristics as the transient case. However, the same conclusions cannot be drawn for NPR 30-50 (RSS).
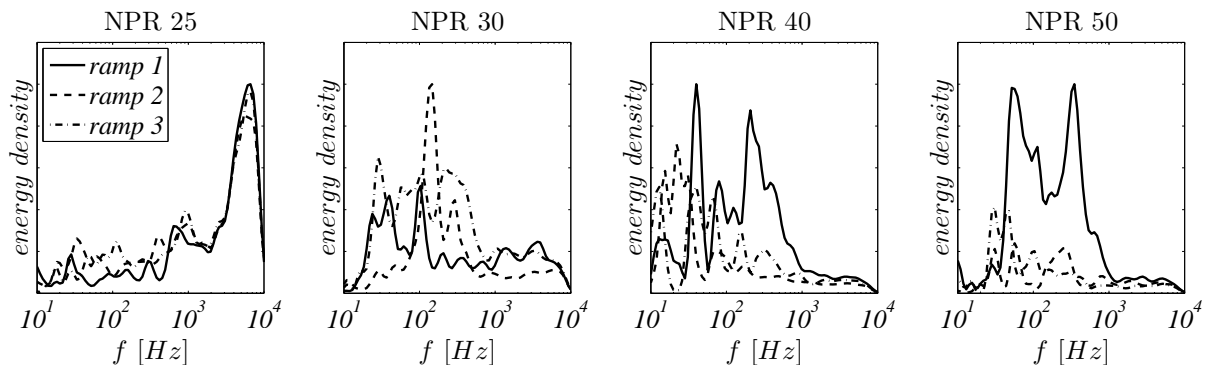

Figure 10. Instantaneous spectra of mode $m = 1$ at axial station x_3, time-averaged from $E(x_3; m = 1; f, t) \cdot f$, for a window size of 2 NPR.
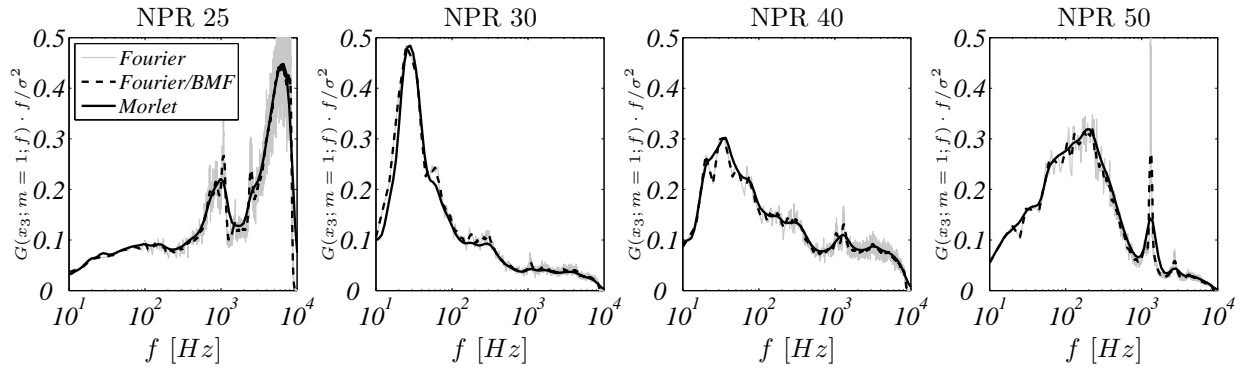
Figure 11. Global wavelet spectra and Fourier spectra during steady operation (both computed from 18s of data) for mode $m = 1$ at axial station x_3.

In summary, it is postulated from these results that the same ramp rate does not necessarily guarantee similar dynamical characteristics. A first order understanding of this filtering would comprise a relationship between the ramping rate time-scale and the time-scales associated with the characteristic frequencies in the flow (Nguyen *et al.*, 2003). An ensemble average over a number of identical transients, though impractical, could converge to unique spectra, thus allowing the effects of dNPR$/dt$ to be more clearly understood. Nevertheless, it appears to be clear from this analysis that a satisfactory understanding of the dynamical characteristics relating to the internal flow and fluctuating wall pressure footprint during transient operation of an overexpanded nozzle can **not** be furnished by way of fixed flow (NPR) analysis. Future work will incorporate synchronized analyses of the fluctuating wall pressure, internal flow and far-field acoustics in order to develop a more complete understanding of the mechanisms responsible for producing these excess vibro-acoustic loads during transient start-up.

References

BAARS, W. J., TINNEY, C. E., RUF, J. H., BROWN, A. M. & McDANIELS, D. M. 2011 Wall pressure unsteadiness and side loads in overexpanded rocket nozzles. *AIAA J. (in print)* .

COHEN, L. 1989 Time-frequency distributions - a review. *Proc. of the IEEE* **77** (7), 941–981.

FARGE, M. 1992 Wavelet transforms and their application to turbulence. *Annu. Rev. Fluid Mech.* **24**, 395–457.

FREY, M. & HAGEMANN, G. 2000 Restricted shock separation in rocket nozzles. *J. of Prop. and Power* **16** (3), 478–484.

HAGEMANN, G., FREY, M. & KOSCHEL, W. 2002 Appearance of restricted shock separation in rocket nozzles. *J. of Prop. and Power* **18** (3), 577–584.

NGUYEN, A. T., DENIAU, H., GIRARD, S. & ALZIARY DE ROQUEFORT, T. 2003 Unsteadiness of flow separation and end-effects regime in a thrust-optimized contour rocket nozzle. *Flow, Turb. and Comb.* **71**, 161–181.

RUF, J. H., McDANIELS, D. M. & BROWN, A. M. 2009 Nozzle side load testing and analysis at Marshall Space Flight Center. In *45th AIAA Joint Prop. Conf*. Denver, CO.